ORIGINAL PAPER

Suitability of superficial electron paramagnetic resonance dosimetry for in vivo measurement and verification of cumulative total doses during IMRT: A proof of principle

Sebastian Höfel[a,b,*], **Michael K. Fix**[c], **Malte Drescher**[a], **Felix Zwicker**[b,d,e]

[a] Department of Chemistry and Konstanz Research School Chemical Biology, University of Konstanz, Germany
[b] Klinik und Praxis für Strahlentherapie am Klinikum Konstanz, Konstanz, Germany
[c] Division of Medical Radiation Physics and Department of Radiation Oncology, Inselspital, Bern University Hospital and University of Bern, Switzerland
[d] Department of Radiation Oncology, Heidelberg University Hospital, Heidelberg, Germany
[e] Clinical Cooperation Unit Molecular Radiation Oncology, German Cancer Research Center (DKFZ), Heidelberg, Germany

Received 24 November 2020; accepted 31 March 2021

Abstract

Purpose: *The present study investigates superficial in vivo dosimetry (IVD) by means of a previously proposed electron paramagnetic resonance (EPR) dosimetry system aiming at measuring and verifying total doses delivered by complex radiotherapy treatments. In view of novel regulatory requirements in Germany, differences between measured and planned total doses to the EPR dosimeters are analyzed and compared to reporting thresholds for significant occurrences.*

Methods: *EPR dosimeters, each consisting of one lithium formate monohydrate (LFM) and one polycrystalline L-alanine (ALA) pellet, were attached to the surface of an anthropomorphic head phantom. Three head and neck treatments with total target doses ranging from 30 to 64 Gy were fully delivered to the phantom by helical tomotherapy. During each treatment, eight EPR dosimeters were placed at distinct spots: (i) within or next to the planning target volume (PTV), (ii) near to organs at risk including the parotid glands and the eye lenses, (iii) at the thyroid lying out-of-field. EPR read out was always performed after all fractions were delivered. EPR results were compared to thermoluminescence dosimeter (TLD) measurements and to the planned total doses derived from the treatment planning system (TPS). Planned total doses to the EPR dosimeters ranged from about 2 to 64 Gy.*

Results: *By taking uncertainties into account, the measured and planned doses were in good agreement. Exceptions occurred mainly at the thyroid (out-of-field) and lenses (extreme sparing). The maximum total dose difference between EPR results and corresponding planned doses was 1.3 Gy occurring at the lenses. Remarkably, each LFM and ALA pellet placed within or next to the PTV provided dose values that were within ±4% of the planned dose. Dose deviations from planned dose values were comparable for EPR and TLD measurements.*

Conclusion: *The results of this proof of principle study suggest that superficial EPR-IVD is applicable in a wide dose range and in various irradiation conditions – being a valuable tool for monitoring cumulative total doses delivered by complex IMRT treatments. EPR-IVD in combination with helical tomotherapy is suitable to reliably detect local dose deviations at superficial dosimeter spots in the order of current national reporting thresholds for significant occurrences (i.e. 10%/4 Gy).*

Keywords: In vivo, EPR dosimetry, Lithium formate, Alanine, Intensity modulated radiotherapy, Tomotherapy

*Corresponding author: Sebastian Höfel, Department of Chemistry. AG Drescher. University of Konstanz, Box 706, Universitätsstraße 10, 78457 Konstanz, Germany.
E-mail: Sebastian.Hoefel@uni-konstanz.de (S. Höfel).

1 Introduction

In vivo dosimetry (IVD) aims to determine actually delivered radiation doses to patients undergoing radiotherapy treatments. IVD is a well-recognized and valuable method being used for different purposes. Primarily, it is applied for ultimate quality assurance in radiotherapy since it allows verification of radiation doses to organs at risk (OAR) and target structures during treatments by comparing measured versus planned doses. By this means and according to international guidelines, IVD complements pretreatment quality checks and verifications by providing an additional and independent safeguard for the detection of errors in the treatment chain [1]. Moreover, IVD can be used in regions lying outside the treatment beams (out-of-field) - even beyond the imaging dataset used for treatment planning, i.e. where no dose values are predicted by the treatment planning system (TPS). The latter situations play an important role e.g. when estimating fetal doses or the risk of secondary cancer induction [2] in the context of radioprotection.

International organizations have been promoting clinical implementation of IVD in radiotherapy [1,3–5], and developed procedures for several point detectors [6,7]. Despite its huge potential for error detection, quality assurance, and accuracy improvements in radiotherapy, however, IVD is not yet mandatory in many countries.

Since recently, the importance of correct dose delivery in radiotherapy is reflected in Germany's national regulatory requirements: In the course of the transposition of the council directive 2013/59/EURATOM [8] into national law, a new radiation protection act [9] and radiation protection ordinance [10] came into force. In this context, a central reporting system for significant occurrences in the medical field has been established on the national level. Significant occurrences include severe deviations of the total delivered dose from the planned dose for both, target volumes and OARs. Dose deviation by more than 10% or 4 Gy are defined as reporting thresholds [10]. Compliance with these regulations requires new efforts and ideas considering the technical realization of monitoring delivered doses in clinical routine. It is expected that these new requirements will strengthen the reasoning in favor of IVD, since it is the only way of reliably determining and documenting actually delivered radiation doses to patients.

So far only little attention was paid to using electron paramagnetic resonance (EPR) dosimetry as an IVD technique – presumably due to the high efforts associated with precise EPR dosimetry protocols based on alanine (ALA). EPR dosimetry offers many advantages for clinical application such as dose response linearity, water equivalence and independence of the detector response regarding beam quality and dose rate [11]. In vivo applications of EPR dosimetry using ALA were first reported during total body irradiations [12,13], and shortly thereafter also in brachytherapy [14,15]. More recently, ALA dosimetry was performed in body cavities during prostate [16] and gynecological [17] external beam radiotherapy (EBRT). Lately, also superficial in vivo application of ALA dosimeters at the contralateral breast during volumetric modulated arc therapy (VMAT) of breast cancer patients was shown [18].

In a previous study [19], we reported on uncertainties of EPR dosimetry using lithium formate monohydrate (LFM) as EPR sensitive material in the radiotherapy dose range by applying a practical dosimetry protocol tailored for routine clinical use in radiotherapy. For LFM, the uncertainties (1σ) were below 3% in the entire dose range between 1 and 70 Gy.

The aim of the current study is to demonstrate the applicability of the proposed EPR dosimetry system as an IVD tool being capable of measuring superficial radiation doses delivered during an entire course of a complex intensity modulated radiotherapy (IMRT) treatment. In order to assess the applicability of LFM dosimeters for future routine IVD during EBRT, the resulting dose values are compared to ALA dosimetry results, to TLD measurements and to the planned dose values based on TPS calculations. Moreover, an uncertainty analysis of measured and planned superficial dose values is performed to assess the reliability of superficial dose verification – especially in view of current reporting thresholds in Germany applying to total dose deviations in radiotherapy.

2 Materials and methods

For illustration purposes, some figures in this chapter were generated by using Eclipse™ radiotherapy treatment planning software version 15.6.6 (Varian, Palo Alto, CA, USA).

2.1 EPR and TLD dosimeter design

Each EPR dosimeter consisted of a cylindrical polypropylene capsule with an outer diameter of 6.4 mm and a length of 12 mm containing two different EPR sensitive pellets: one ALA and one LFM pellet as shown in Figure 1(a). The EPR sensitive pellets had a cylindrical shape with a diameter of 4 mm and a height of 2 mm (ALA) or 4 mm (LFM). Synthetic rubber plugs (black part in Figure 1(a)) were used to fix the pellets positions inside the capsule and to close the capsules at the end. Further details regarding dosimeter preparation are provided in [19].

Lithium fluoride (LiF) TLD detectors (TLD-100) were received from PTW Freiburg GmbH (Freiburg i. Br., Germany). Each TLD detector consisted of a cylindrical TLD chip (diameter of 4 mm, height of 1 mm) that was encapsulated in a cylindrical polymethyl methacrylate (PMMA) rod with a length of 2.5 cm and a diameter of 5 mm. All TLD chips were exactly located in the center of the PMMA rods.

2.2 Phantom, dosimeter placement and CT acquisition

The dosimeters were placed at distinct positions (hereinafter referred to as spots) located on the surface of an

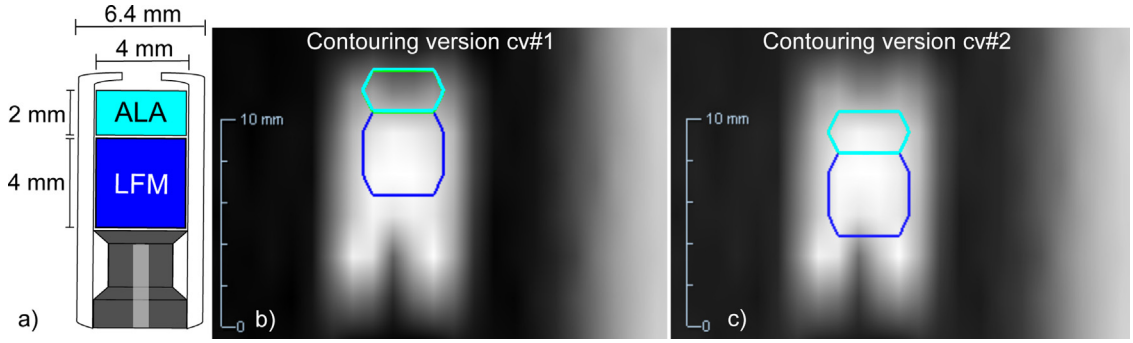

Figure 1. Cross-sections parallel to the EPR dosimeters' symmetry axis. Sketch and dimensions of EPR dosimeter design (a). Exemplary coronal view of an EPR dosimeter's representation in the planning CT image and the two most appropriate contouring versions cv#1 (b) and cv#2 (c) for the ALA and LFM pellets. ALA and LFM contours are shown in cyan and dark blue colors, respectively.

Table 1
Summary and comparison of the investigated irradiation scenarios.

Irradiation scenarios	Labels	SC#1	SC#2	SC#3
Treatment case		WBRT	WBRT	OROPH
Prescribed dose		30 Gy in 10 fractions	30 Gy in 10 fractions	64 Gy in 32 fractions (SIB) 57.6 Gy in 32 fractions (PTV)
Normalization		D_{50}(PTV) = 30 Gy	D_{50}(PTV) = 30 Gy	D_{50}(PTV) = 57.6 Gy
OARs		Parotid glands, eyes, eye lenses, mandibular joints, thyroid	Parotid glands, eyes, eye lenses, mandibular joints, thyroid	Parotid glands, eyes, eye lenses, mandibular joints, thyroid, spinal cord
Dosimeter spots (special conditions)	TaR	Right forehead	Right forehead	Chin (5 mm bolus)
	TaL	Left forehead (5 mm bolus)	Left forehead (5 mm bolus)	Chin (5 mm bolus)
	PaR	Next to right parotid gland		
	PaL	Next to left parotid gland		
	LeR	Next to right eye lens		
	LeL	Next to left eye lens (complete beam blocking)		
	ThR	Next to right thyroid lobe (about 2–3 cm from caudal field edge)		
	ThL	Next to left thyroid lobe (about 2–3 cm from caudal field edge)		
Total treatment time period		1 h	1.5 h	6 weeks
Positioning of EPR dosimeters		Exactly as planned for all fractions	Repositioned in between fractions	Repositioned in between fractions
Positioning of phantom		Once initially according to laser markings	Once initially according to laser markings	Repositioned in between fractions according to laser markings

anthropomorphic head phantom (Alderson phantom, RSD Phantoms, CA, USA): either within or next to target structures or close to OARs.

Three different irradiation scenarios (SC#1-3) are investigated (cf. Table 1 and Section 2.4). For each scenario, eight dosimeter spots were defined and labeled as illustrated in Figure 2. The labels reflect the associated anatomical structures: lenses (Le), parotid glands (Pa), target (Ta) and thyroid (Th). As seen in Figure 2, the third letter indicates the left(L)/right(R) side of the phantom. The dosimeter spots for scenarios SC#1 and SC#2 were the same. In scenarios SC#1/SC#2, TaL is located between the phantoms left forehead and a 5 mm bolus, while in scenario SC#3 the target dosimeters TaR and TaL are located underneath a 5 mm bolus at the phantom's chin.

All dosimeter spots were marked with velcro strips on the phantom's body. Corresponding velcro stickers were attached to the EPR as well as the TLD dosimeters in order to place them within a maximum isotropic deviation of ±2 mm from the indented position.

For both detector types, great care was taken that the dosimeters' symmetry axis was always in parallel with the *y*-direction according to the International Electrotechnical Commission (IEC) accelerator coordinate system.

Computed tomography (CT) datasets were acquired for treatment planning using a SOMATOM® Definition Flash

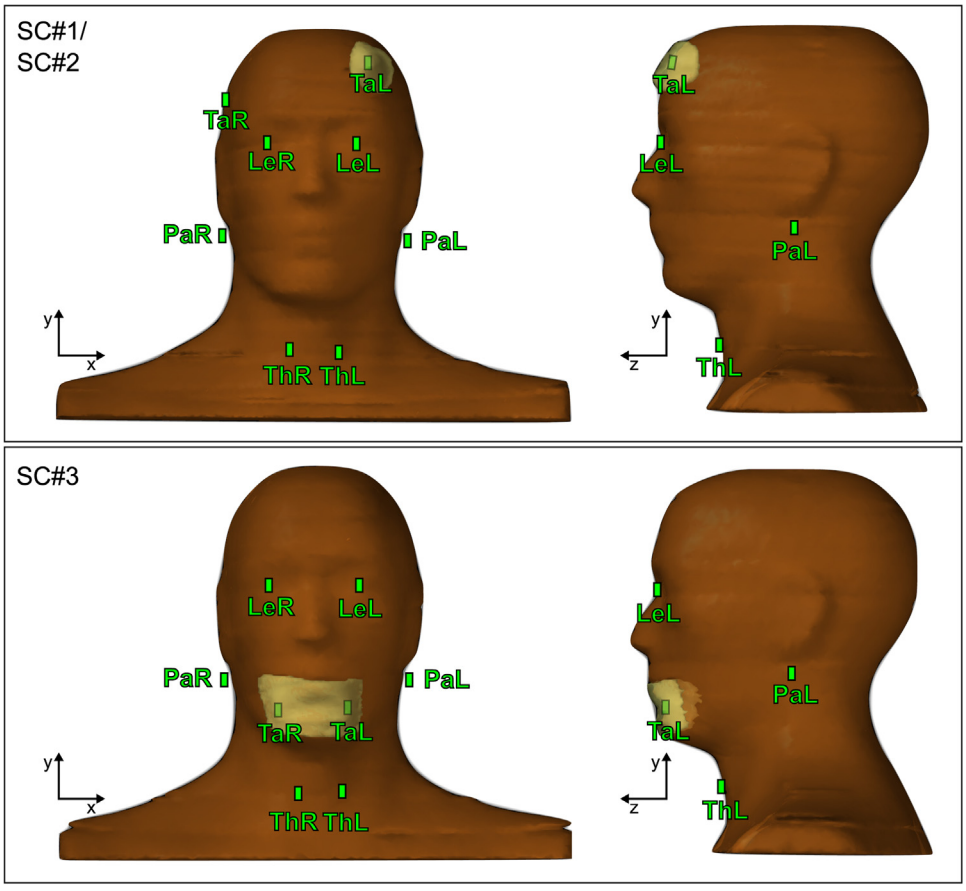

Figure 2. Superficial dosimeter placements (green spots) on the phantom's body (brown surface) for irradiation scenarios SC#1/SC#2 (top) and SC#3 (bottom). Dosimeter labels shown in green (target (TaR/TaL), parotid glands (PaR/PaL), eye lenses (LeR/LeL), thyroid (ThR/ThL)) and bolus material in translucent yellow. Definition of the phantom position in relation to the IEC coordinate system.

(Siemens Healthcare, Erlangen, Germany) CT scanner. Image reconstruction was performed by applying filtered back projection with a conventional kernel (B31s) and 2 mm slice width. In total, four CT scans of the phantom were performed: Two for each dosimeter setup shown in Figure 2 (SC#1/SC#2 or SC#3) with either eight EPR or eight TLD dosimeters attached. The two CT datasets showing the EPR dosimeters were used as primary CTs during treatment planning whereas the CT datasets with TLDs served for dose re-calculation (cf. Section 2.5).

2.3 Treatment planning

For either dosimeter setup shown in Figure 2, a complex head and neck treatment plan was created using helical Tomotherapy (Accuray Inc., Sunnyvale, CA, USA).

The first treatment plan (WBRT) was created for irradiations scenarios SC#1 and SC#2 and simulates a whole-brain radiotherapy including subcutaneous and bone metastases. The inferior field border was extended to the sixth cervical vertebra of the spine. The planning target volume (PTV) included a fictitious subcutaneous metastasis at the left forehead – where the 5 mm bolus and target dosimeter TaL was applied (Figure 2). A helical tomotherapy plan was created with the following settings: Longitudinal field width of 5 cm (dynamic jaw mode), pitch of 0.297 and planning modulation factor of 2.0. A total median dose of 30 Gy in 10 fractions (3.0 Gy single fraction dose) was prescribed to the PTV. Plan normalization was set accordingly to $D_{50}(PTV) = 30$ Gy.

The second treatment plan was created for irradiation scenario SC#3 following a clinical case of a ventral floor of mouth cancer (OROPH) with infiltration of the ventral mandible and lips. A helical tomotherapy plan was created with the following settings: Longitudinal field width of 5 cm (dynamic jaw mode), pitch of 0.297 and planning modulation factor of 2.4. A total median dose of 57.6 Gy in 32 fractions (1.8 Gy single fraction dose) was prescribed to the PTV which extended from the base of the skull to the hyoid bone in craniocaudal direction. Plan normalization was set accordingly to $D_{50}(PTV) = 57.6$ Gy. The PTV completely encompassed the oropharynx and the lymph node levels I and II. A simultaneous integrated boost (SIB) was defined in the oral cavity

as a sub-volume of the PTV. The SIB volume was extended ventrally to include the lips, parts of the 5 mm bolus material and two EPR dosimeters. The planned median dose in the SIB volume was 63.9 Gy.

For both treatment plans, the following OARs located in-field were contoured and considered during optimization: eyes, eye lenses, parotid glands and mandibular joints. The thyroid was contoured as well, but was located inferior to the caudal field border (out-of-field). In the OROPH case, the spinal cord was considered as OAR additionally.

Note that the exact structure of the eyes, eye lenses, parotid glands and the thyroid were not identifiable in the phantom's CT. Therefore, OAR contouring was rather based on experience than on visible structures.

In both cases, the thyroid dosimeter spots were located out-of-field, i.e. about 2–3 cm from the inferior edge of the PTV.

The mean doses to the eye lenses and the respective dosimeter spots were pushed below 6 Gy during optimization of both plans. Additionally, the left lens and dosimeter LeL were completely blocked by the collimator system, i.e. no primary photon fluence passed through these regions. Corresponding binary leafs of the multileaf collimator (MLC) were automatically closed.

Dose calculation was performed using Accuray's Precision 2.0.1.1 (Accuray Inc., Sunnyvale, CA, USA) TPS. Both, the CT voxel matrix and the calculation grid had an axial spatial resolution of 1 mm (IEC x–z-plane). In IEC y-direction, the dose grid had a spatial resolution of 2 mm corresponding to the CT slice thickness.

2.4 Irradiation scenarios

Phantom irradiations were performed using a clinical Tomotherapy Hi-Art® treatment machine (Accuray Inc., Sunnyvale, CA, USA). The tomotherapy machine is calibrated against the TPS following the concept of plan-class specific reference fields [20,21]. The same ionization chamber was used for calibration of machine output and calibration of the EPR dosimetry system [19].

Three different irradiation scenarios were applied to the EPR dosimeters. A summary and comparison is given in Table 1.

Irradiation scenarios SC#1 and SC#2 were conducted by applying all fractions of treatment plan WBRT. In scenario SC#1, the EPR dosimeters were not repositioned in between fractions, but were left exactly at the same location in relation to the phantom surface as during acquisition of the planning CT. Before the first fraction, the phantom was positioned on the treatment couch according to superficial markings for the in-room laser system as defined in the treatment plan. The phantom stayed in this initial position during the delivery of all fractions.

SC#2 was conducted right after SC#1. The only difference between SC#1 and SC#2 was that the EPR dosimeters were removed and straightaway re-attached to the respective dosimeter spot between fractions.

Irradiation scenario SC#3 mimicked a realistic fractionated head and neck treatment extending over a treatment period of more than 6 weeks (32 fractions) and including repositioning of the dosimeters as well as repositioning of the phantom in between fractions. Before each fraction, the phantom was positioned on the treatment couch as planned according to superficial markings for the in-room laser system.

In contrary to clinical practice, no daily image guidance via megavoltage CT (MVCT) was performed, since correct positioning of the rigid phantom was considered to be reproducible within an isotropic tolerance of ± 1 mm by means of the laser system and, moreover, the imaging dose is not considered in the total dose calculation of the TPS.

All EPR dosimeters were irradiated at room temperature (20–25 °C). Before and after irradiation, the EPR dosimeters were stored in an air-tight box that provided a constant level of $34 \pm 2\%$ relative humidity.

For an independent dosimetry check, TLD detectors were used to measure single fraction doses to the dosimeter spots. TLD irradiations were performed for both treatment plans. A minimum of three fractions were delivered, each to a different set of TLD detectors.

2.5 Planned dose determination

Planned doses to the EPR pellets were derived from TPS calculations as follows. For each EPR dosimeter, ALA and LFM pellets were contoured separately with a diameter of 4 mm on the primary CT. Due to the finite CT slice thickness (2 mm) and the resulting partial volume artefacts, two contouring versions (cv#1 and cv#2) were chosen to capture the pellets' true position. An example is shown in Figure 1(b) and (c). Each pellet i was thus represented by two structures ($S_i^{vc\#1}$, $S_i^{vc\#2}$). After final dose calculation, mean dose values D_m within the pellet structures for both contouring versions ($D_m(S_i^{vc\#1})$, $D_m(S_i^{vc\#2})$) were extracted from the dose statistics table of the TPS. For each pellet, the planned dose D^p was defined as the mean value of the mean doses calculated within the two associated structures ($D^p = mean\{D_m(S_i^{vc\#1}), D_m(S_i^{vc\#2})\}$). The absolute half of the difference between the two mean dose values ($1/2|D_m(S_i^{vc\#1}) - D_m(S_i^{vc\#2})|$) was taken as uncertainty component for contouring (cf. Section 2.7).

An equivalent procedure was performed for the TLD chips using the secondary CT dataset. After contouring, the secondary CT was registered to the primary CT. The treatment plan was then applied to the secondary CT, i.e. the dose distribution was re-calculated. Planned dose values were determined as described above.

2.6 Dose measurements

EPR measurements were performed on a compact benchtop spectrometer (MiniScope MS 5000, Magnettech by Freiberg

Instruments GmbH, Freiberg, Germany) immediately after all fractions were delivered. Each pellet was measured for 10 min. A detailed description of the measuring and evaluation procedure is presented in a previous study [19]. Since the EPR dosimeters were irradiated at room temperature (as the dosimeters used for calibration) no additional temperature correction was applied.

For the EPR dosimeters irradiated over a period of about 6 weeks (SC#3), fading correction was considered. In order to account for fading, it was assumed that the EPR dosimeters were irradiated at a specific date lying in the middle between the first and the last day of treatment. For the ALA pellets, a fading correction factor of 1.0026 was calculated and applied (fading rate is about 3% per year). Regarding the LFM dosimeters, fading affects not only the signal amplitude but also the line shape of the EPR spectrum. A fading correction was inherently considered during spectral evaluation by choosing the appropriate LFM base spectrum (week 5) from the set of available base spectra [19].

Absorbed dose values at the dosimeter spots were also obtained via TLD irradiations (Section 2.4). The irradiated TLDs were immediately evaluated by PTW Freiburg GmbH taking beam quality correction (6 MV) into account. For each dosimeter spot, the results of minimum three irradiated TLDs were averaged. Unlike in the case of the EPR measurements, the TLD mean values reflect the dose delivered during one single fraction. For direct comparison with the planned total dose values and the EPR results, the TLD mean values were multiplied by the respective number of total fractions.

The irradiation conditions investigated in this work (dose build-up region, complex helical IMRT plan) are considerably different from typical reference conditions and the conditions applied for the calibration of the EPR dosimeters (10 cm depth, fixed beam, etc.) [19]. Hence, the dose response of ALA-EPR, LFM-EPR and LiF-TLD detectors might change when applied on the surface or in shallow depths (e.g. underneath 5 mm bolus). In order to assess possible changes in the detector response, Monte Carlo (MC) simulations were performed using the Geant4 [22] toolkit and a validated phase-space file for the tomotherapy beam [23,24]. In the simulation geometry, EPR and TLD dosimeters as defined in Section 2.1 were placed next to the surface of a water phantom. The dosimeters' responses at the surface $(D_{Dosimeter}/D_{H2O})^{Surface}$ (for various angles of beam incidence) in relation to the dosimeters' responses under reference conditions $(D_{Dosimeter}/D_{H2O})^{Ref}$ were investigated. For each dosimeter material, the ratios $(D_{Dosimeter}/D_{H2O})^{Surface}/(D_{Dosimeter}/D_{H2O})^{Ref}$ were averaged over all beam incidence angles resulting in surface correction factors $k_{Surface}$ for complex irradiation scenarios. The surface correction factors including standard uncertainties were $k_{Surface,ALA} = 0.991(5)$ for ALA, $k_{Surface,LFM} = 0.990(7)$ for LFM and $k_{Surface,LiF} = 0.996(27)$ for LiF. Although relative corrections were determined to be very small (<1%), the surface correction factors were applied to the respective measurement results. Moreover, an additional uncertainty contribution due to surface application was taken into account (cf. Table 2 and Section 2.7).

2.7 Uncertainty considerations

Uncertainties in this work are determined and expressed in accordance with the Guide to the Expression of Uncertainty in Measurement published by the International Organization for Standardization [25]. Unless otherwise stated, all uncertainties are to be seen as type B standard uncertainties (1σ), i.e. the stated standard uncertainties are based on previous measurements, scientific judgement or experience.

Uncertainty budgets for the planned dose and the measured doses values (EPR and TLD) are summarized in Table 2.

For the planned dose (cf. Section 2.5), the following uncertainty components were considered: (i) estimated dose uncertainty of 0.5% emerging from the uncertainty of the CT's hounsfield units (HU), (ii) uncertainty of the beam model beyond the dose build-up region (0.5%), i.e. mean deviation between measured and modeled depth dose curves and beam profiles. Based on the tomotherapy out-of-field dose accuracy study of Schneider et al. [26], an increased uncertainty of 5% was attributed to locations receiving a small fraction of the prescribed dose (2–30% of the prescribed dose), i.e. the dosimeter spots lying out-of-field (ThL and ThR) or in regions where primary beam incidence was considerably suppressed due to OAR sparing (PaL, PaR, LeL, LeR), (iii) additional uncertainty of tomotherapy's convolution/superposition dose calculation algorithm in the build-up region (2.0% assumed), (iv) output fluctuations of the treatment machine (based on daily ionization chamber measurements). For the target spots TaL and TaR, the combined uncertainty of the TPS was estimated to be 2.2% (5.4% for the other dosimeter spots lying predominantly out of the primary beam).

An additional uncertainty due to contouring of the dosimeter pellets as described in Section 2.5 was taken into account.

The determination of relative measurement uncertainties for the EPR method was described in a previous study [19]. Due to less controlled conditions during superficial in vivo applications, an additional uncertainty contribution of 0.2% regarding temperature effects is taken into account in the current study. In addition, uncertainties of the fading correction procedure were estimated to 0.1% (ALA) and 0.3% (LFM). For dose measurements in the build-up region, an extra uncertainty component of the surface correction factor had to be taken into account (cf. Section 2.6).

The dose accuracy of the TLD results were stated by PTW as 1.5% for single fraction doses above 150 mGy and 2.5% for doses below 150 mGy. As for EPR, an additional uncertainty contribution needs to be considered when TLDs are applied in the dose build-up region. Based on MC simulations, this uncertainty contribution is considerably higher for LiF-TLD (2.7%) compared to EPR (0.5% ALA, 0.7% LFM).

Table 2
Uncertainty budgets for calculation based planned dose values and measured dose values given as relative standard uncertainties (1σ).

Uncertainty budgets				
Planned dose		Dose measured by	EPR	
			ALA	LFM
Component	Rel. standard uncertainty [%]	Component	Rel. standard uncertainty [%]	Rel. standard uncertainty [%]
HU uncertainty	0.5	Fading	0.1	0.3
Beam model basic data (out of primary beam)	0.5 (5.0)	Irradiation temperature	0.2	0.2
Dose calculation in build-up	2.0	Application in dose build-up	0.5	0.7
Output fluctuations of the treatment machine	0.5	EPR measurement result including pellet mass at 2/5/10/ 20/30/60 Gy	6.5/2.6/1.3/ 0.7/0.5/0.4	1.7/0.9/0.6/ 0.5/0.5/0.5
Combined uncertainty for TPS dose (out of primary beam)	2.2 (5.4)	Total combined uncertainty for EPR at 2/5/10/ 20/30/60 Gy	6.5/2.7/1.4/ 0.9/0.7/0.7	1.9/1.2/1.0/ 0.9/0.9/0.9
Additional contributions: Contouring of the pellets	Specific to each pellet (see text)	Dose measured by	TLD	
			LiF	
Ranges (min. . . . max.) for the total combined uncertainty of the planned dose	ALA: (2.2 . . . 22.0)	Component	Rel. stand. uncertainty [%]	
	LFM: (2.2 . . . 18.2)	Dose corrected for 6 MV beam as stated by PTW	2.5 (below 150 mGy/fraction) 1.5 (above 150 mGy/fraction)	
	LiF: (2.2 . . . 7.6)	Application in dose build-up	2.7	
	cf. Table 4	Total combined uncertainty for TLD	**3.7** (below 150 mGy/fraction) **3.1** (above 150 mGy/fraction)	

The total combined uncertainties given in Table 2 were obtained by calculating the square-root of the sum of the single squared uncertainty contributions.

Planned doses (D^p, Section 2.5) and measured doses (D^m, Section 2.6) obtained in this work are estimations of the actually delivered doses to the dosimeters. The planned dose neglects the uncertainty of repositioning of the dosimeters in relation to the phantom surface (SC#2, SC#3) and positioning of the phantom in relation to the treatment beam (for all scenarios).

The combined uncertainty $u_c(\Delta D)$ of the dose difference $\Delta D = D^m - D^p$ is calculated via $u_c(\Delta D)^2 = u_c(D^p)^2 + u_c(D^m)^2$.

3 Results

Figure 3 shows the locations of the superficial dosimeter spots in relation to the planned dose distributions of the applied head and neck irradiation scenarios (SC#1-3) described in Table 1. Total planned doses to the contoured OARs are given in Table 3.

As can be seen in Figure 3, the dosimeters were placed in different irradiation situations: Within or next to the PTV (TaL,TaR), next to OARs located in-field (eye lenses: LeL, LeR; parotid glands: PaL, PaR) or out-of-field (thyroid: ThL, ThR).

Planned (D^p) and measured (D^m) total dose values in combination with absolute standard uncertainties (Section 2.7) for all dosimeter spots and irradiation scenarios are listed in Table 4. Agreement between measured and planned dose values can be assessed from the overlapping of uncertainty margins (1σ). According to this criterion, agreement between measured and planned doses is observed for both, EPR and TLD dosimeters at the target (TaR and TaL), thyroid (ThR and ThL) and parotid (PaR and PaL) spots. Some exceptions occurred which are underlined in Table 4. Note that none of the measured dose values at the eye lenses (LeL and LeR) were in agreement with the planned dose.

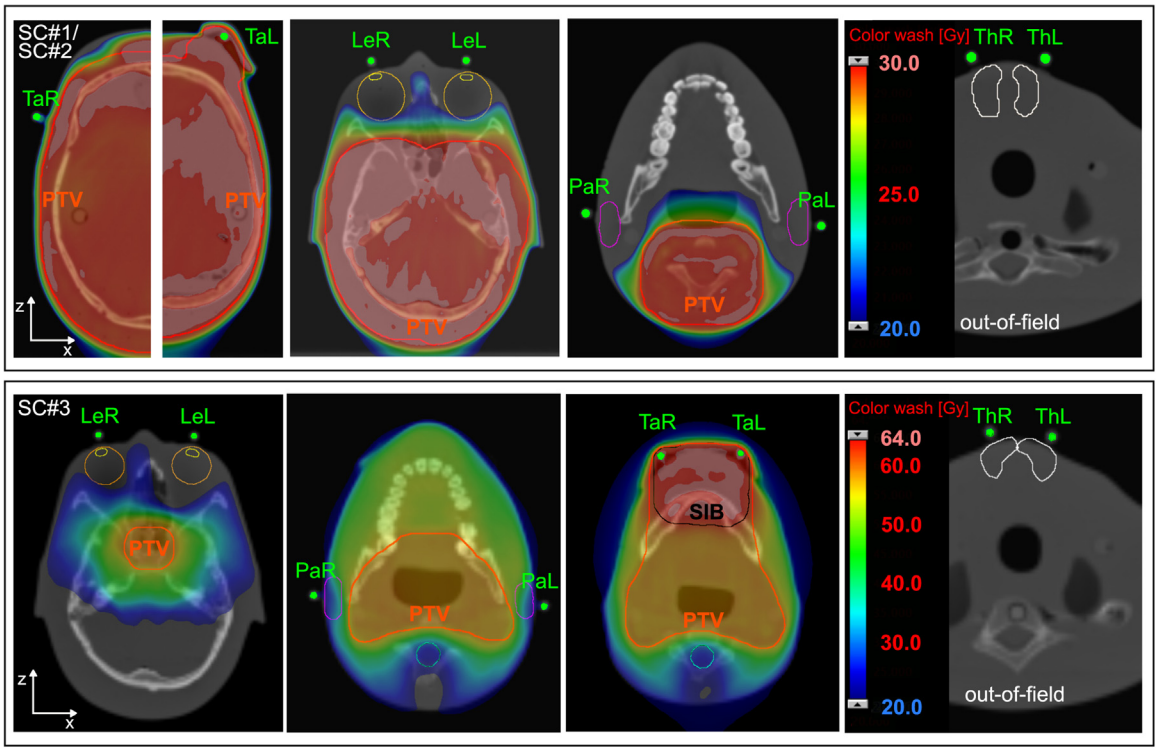

Figure 3. Axial views of the calculated dose distribution superimposed on the corresponding primary CT slices illustrating the dosimeters' locations for the irradiation scenarios SC#1/SC#2 (top) and SC#3 (bottom). Dosimeter spots and corresponding labels are shown in green. Contours of target structures (PTV (orange), SIB (black)) and OARs (lenses (yellow), parotid glands (pink), spinal cord (cyan) and thyroid (white)) are displayed. The thyroid was located outside the primary beam (out-of-field).

Table 3
Planned total doses to OARs: Eyes, eye lenses, mandibular joints (MJ), parotid glands (PG), thyroid and spinal cord.

Irradiation scenarios	SC#1/SC#2	SC#3
Treatment	WBRT	OROPH
	Mean OAR dose [Gy]	
Eye L	10.6	2.2
Eye R	12.0	10.7
Lens L	2.5	1.7
Lens R	3.9	5.8
MJ L	25.8	36.9
MJ R	26.8	35.2
PG L	12.2	24.9
PG R	11.9	25.0
Thyroid	3.4	2.0
Spinal cord	–	33.6 (Max)

Differences between measured and planned dose values at each dosimeter spot and for each dosimetry technique (ALA-EPR, LFM-EPR and LiF-TLD) are illustrated in Figure 4. The dose differences $D^m - D^p$ are shown in absolute as well as relative terms with respect to the planned dose. Uncertainty margins for the dose difference (Section 2.7) are indicated by the error bars.

Looking at all EPR measurements, absolute dose differences $D^m - D^p$ were always below 1.3 Gy (observed with ALA for spot LeR in irradiation scenario SC#2).

With regard to using EPR dosimetry for treatment verification, the dose differences and the associated combined uncertainties at the target spots are of special interest. At these spots, the maximum absolute dose difference $D^m - D^p$ was 1.15 Gy (SC#3, TaL) for ALA and 0.88 Gy for LFM (TaR, SC#2). In relative terms, the dose differences were 1.8% (ALA, TaL, SC#3) and 4.0% (LFM, TaR, SC#2). Except for TaR in SC#2, the error bars in Figure 4 cover the zero-difference line, i.e. the observed dose differences at the target spots were mostly within uncertainties (1σ).

At the parotid spots (PaL and PaR), the TPS systematically underestimated the dose by about 0.25 Gy (SC#1/SC#2) and 0.5 Gy (SC#3). However, the observed dose underestimation was still within uncertainty margins. Expressed in relative terms, this dose underestimation is approximately 4% (SC#1/SC#2) or 2.5% (SC#3) of the planned dose at the parotid spots and about 0.8% of the respective prescribed dose.

More reliable dose differences $D^m - D^p$ are observed at the lens spots (LeR and LeL). At these locations, the uncertainty margins (1σ) for measured and planned doses did not overlap (cf. Table 4). As for the parotid spots, an underestimation of the TPS dose was observed (cf. Figure 4). It amounts up to

Table 4
Comparison of planned doses D^p versus measured doses D^m for each irradiation scenario and dosimeter spot. Respective combined uncertainties u_c are given in brackets as absolute standard uncertainties (1σ). Underlined numbers mark observations for which the uncertainty margins of planned and measured values do not overlap.

	Spot	ALA-EPR		LFM-EPR		LiF-TLD	
		$D^p(u_c)$ [Gy]	$D^m(u_c)$ [Gy]	$D^p(u_c)$ [Gy]	$D^m(u_c)$ [Gy]	$D^p(u_c)$ [Gy]	$D^m(u_c)$ [Gy]
SC#1/ SC#2							
	TaL	29.95(0.66)	29.55(0.23)/ 29.52(0.23)	30.03(0.66)	29.95(0.27)/ 29.65(0.27)	30.04(0.67)	30.48(0.94)
	TaR	21.41(0.51)	21.53(0.19)/ 22.03(0.19)	21.70(0.50)	22.18(0.21)/ 22.58(0.21)	23.08(0.51)	24.20(0.75)
	PaL	6.53(0.37)	6.57(0.14)/ 6.65(0.14)	6.68(0.36)	6.96(0.07)/ 6.87(0.07)	6.84(0.40)	7.28(0.23)
	PaR	6.49(0.35)	6.63(0.14)/ 6.73(0.14)	6.59(0.36)	6.87(0.07)/ 6.97(0.07)	6.62(0.37)	7.07(0.22)
	LeL	3.03(0.35)	3.65(0.13)/ 3.53(0.13)	2.56(0.20)	3.14(0.05)/ 2.99(0.04)	2.36(0.18)	2.89(0.09)
	LeR	4.96(0.29)	5.91(0.13)/ 6.25(0.14)	4.50(0.29)	5.65(0.06)/ 5.66(0.06)	4.54(0.29)	5.58(0.17)
	ThL	1.32(0.29)	1.61(0.13)/ 1.40(0.13)	0.97(0.11)	1.24(0.03)/ 1.12(0.03)	0.92(0.07)	1.01(0.04)
	ThR	1.76(0.38)	1.94(0.13)/ 1.64(0.13)	1.10(0.20)	1.29(0.03)/ 1.16(0.03)	1.00(0.06)	1.11(0.04)
SC#3							
	TaL	64.54(1.42)	65.69(0.44)	64.51(1.42)	64.20(0.59)	65.02(1.43)	66.54(2.06)
	TaR	64.53(1.42)	63.50(0.43)	64.51(1.42)	64.21(0.59)	64.59(1.42)	64.32(1.99)
	PaL	19.33(1.12)	19.64(0.18)	19.56(1.06)	20.17(0.19)	20.25(1.10)	20.69(0.64)
	PaR	20.13(1.13)	21.04(0.19)	19.22(1.12)	19.92(0.19)	20.49(1.13)	21.68(0.67)
	LeL	1.58(0.09)	2.37(0.13)	1.51(0.08)	2.17(0.04)	1.64(0.09)	2.09(0.08)
	LeR	4.93(0.28)	6.03(0.14)	4.63(0.27)	5.33(0.07)	4.94(0.32)	5.47(0.17)
	ThL	2.12(0.13)	2.32(0.13)	3.08(0.40)	3.11(0.05)	2.15(0.16)	2.19(0.08)
	ThR	3.64(0.57)	3.90(0.13)	2.42(0.20)	2.65(0.05)	2.22(0.16)	2.21(0.08)

1.3 Gy for LeR in SC#2. In relation to the prescribed dose, the dose differences observed at the lens spots were in the order of 4% or below. With respect to the planned dose at the lens spots, however, the relative dose difference is considerable (up to 50%, e.g. LeL in SC#3).

No clear systematic dose under- or overestimation was observed for the thyroid spots. Relative combined uncertainties for the dose difference were highest for the thyroid spots, since the thyroid dosimeters were located out-of-field (about 2–3 cm from the inferior field border, i.e. still within considerable relative dose gradients in IEC y-direction) and the gradient strength in y-direction is reflected in the contouring uncertainty contribution (Section 2.5). Although considerable relative deviations from the planned dose were observed (e.g. 28% for LFM at ThL in SC#1), the differences were still within uncertainties in most cases.

Three main observations result from Figure 4. Firstly, the observed absolute dose differences between EPR measurements and the planned dose are small (<1.3 Gy) and combined uncertainties (1σ) for the dose difference $D^m - D^p$ were always below 1.6 Gy. Secondly, by taking uncertainty margins into account, the dose differences $D^m - D^p$ observed for LFM and ALA at each dosimeter spot are consistent with each other. Similarly, the dose differences observed with EPR dosimetry are in agreement with the respective TLD results. One exception occurred at spot LeL in SC#3. Thirdly, the EPR measurements of both pellet types as well as the TLD measurements at the lens spots were significantly higher than the respective planned dose suggesting some limitations of the TPS dose calculation algorithm for these irradiation conditions. Good agreement, however, is found for the target spots – within ±4% of the planned dose.

4 Discussion

Different irradiation scenarios (Table 1 and Figure 3) with total doses to the dosimeters ranging from about 2 to 64 Gy were investigated and a detailed uncertainty analysis for the measured and planned dose values was performed (Table 2 and Table 4 and Figure 4).

By taking uncertainty margins into account, the differences between measured and planned doses at each dosimeter spot were comparable for EPR and TLD dosimetry. Evaluation of the TLDs was performed externally by the German secondary standard dosimetry laboratory at PTW Freiburg GmbH. TLD dose values were considered as ground truth and served as

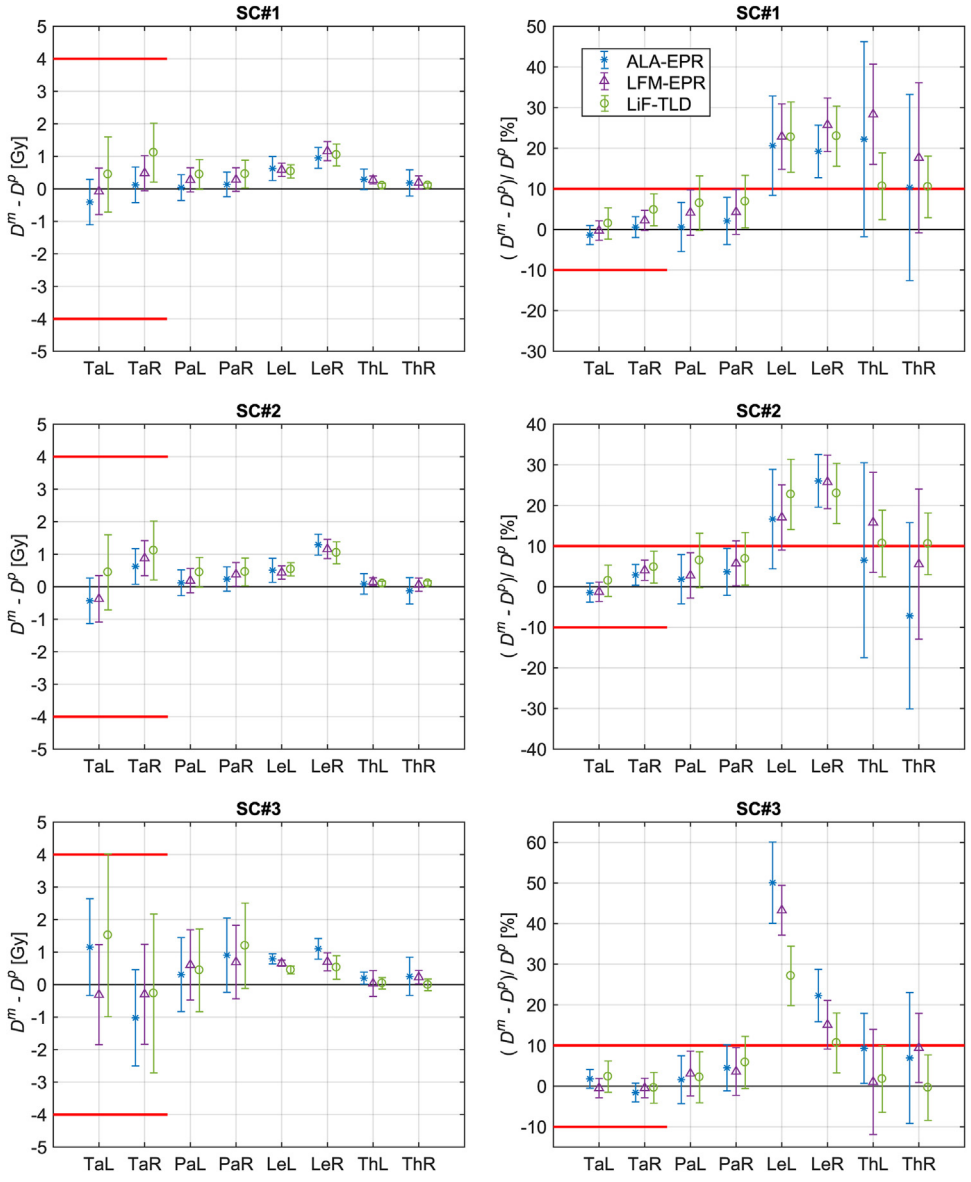

Figure 4. Absolute (left) and relative (right) local dose differences between measured and planned total dose values for irradiation scenarios SC#1 (top), SC#2 (middle) and SC#3 (bottom). For comparison, results of ALA-EPR (blue stars), LFM-EPR (purple triangles) and LiF-TLD (green circles) are grouped for each dosimeter spot. Combined uncertainties (1σ) of the dose difference are represented by error bars. Reporting thresholds (10%/4 Gy) are indicated by red horizontal lines.

an independent check for the EPR-IVD procedure. Based on the TLD comparison, the applied EPR-IVD procedure has proven to be reliable and suitable. During the analysis, material dependent surface correction factors with corresponding uncertainties resulting from MC simulations were considered (Section 2.6). Relative corrections for superficial application were small (<1%) in relation to the established uncertainties (see Table 4 and Figure 4). Due to the good agreement observed between the measured values at each dosimeter spot (Figure 4), these correction values are supported by the experimental results of this work. Further support is found in the literature. A previously reported value of the surface correction factor for ALA is $k_{Q,in\text{-}vivo} = 0.988(10)$ [18], which is in good agreement with the correction factor presented in this work. Besides, it was shown experimentally that the dependence of the EPR response on dose rate [27,28], and beam quality [29,30], is of minor importance for therapeutic beams.

All phantom irradiations were successfully performed as specified by the applied treatment plans. The planned total doses at the dosimeter spots derived from TPS calculations should ideally match the actually delivered dose at these

locations, especially in scenario SC#1 where the dosimeters' positions during irradiation exactly matched the planned situation. For SC#2 and SC#3, deviations were expected, since the dosimeters were repositioned between fractions. In SC#3, not only the dosimeters but also the phantom was repositioned between fractions mimicking a realistic head and neck treatment. Concerning verification of planned doses by superficial IVD measurements, two questions arise: (i) How large are the differences between measured and planned total doses at the dosimeter spots for ideal (SC#1) and more complex (SC#2, SC#3) treatment scenarios, (ii) are the determined differences still within uncertainty margins and how large are the uncertainty margins compared to the desired accuracy level. The underlying primary question is, however, whether the dose calculation algorithm of the TPS fulfills high levels of accuracy at the superficial dosimeter spots (dose build-up region).

By taking uncertainties into account, agreement between measured and planned dose values was found for all target dosimeters placed underneath a 5 mm bolus (TaR and TaL in SC#3, TaL in SC#1 and SC#2). Agreement was also found for the EPR results at spot TaR (no bolus) in SC#1. In SC#2, the EPR dosimeters were repositioned between fractions leading to an increased dose difference at spot TaR. The results demonstrate that a relative combined uncertainty of only 2.2% for tomotherapy's dose calculation in the build-up region is justifiable and that the agreement between measured and planned target doses is more robust, when 5 mm bolus is applied.

Apart from the target spots, agreement between measured and planned dose values was observed for the parotid spots in all scenarios, even though a small overall dose difference was observed. These results show the feasibility of superficial total dose verification by EPR-IVD next to OARs without the use of additional bolus.

As can be seen in Figure 4, the dose differences and the corresponding uncertainties for the target and parotid spots are smaller than current reporting thresholds for significant occurrences [10]: For target volumes, deviations of ±10% from the planned mean dose has to be reported. Also local dose deviations of ±10% with respect to the planned dose within target structures are subject to mandatory reporting as long as the absolute value of the dose difference exceeds 4 Gy. For OARs, reporting thresholds relating to mean OAR doses lie 10% above the respective planned mean dose or 10% above the dose constraint defined in the institution's standard operating procedures. The red horizontal lines in Figure 4 indicate reporting thresholds when these criteria are translated to the planned dose values at the dosimeter spots. The EPR measurements at the target and parotid spots showed a maximum deviation of 4% and 1.15 Gy with respect to the planned dose. The uncertainties (1σ) for the dose difference did not exceed 1.54 Gy and 6% in absolute and relative terms, respectively. The observed dose differences and corresponding uncertainties for EPR-IVD are small compared to the (10%/4 Gy) criterion. Dose deviations to superficial dosimeter spots by more than 10%/4 Gy can thus be reliably detected. Superficial EPR-IVD could be used as an additional safeguard monitoring total doses to target as well as superficial OAR structures (e.g. the parotid glands): Severe dose deviations at the dosimeters spots may prompt further investigations whether the criteria for reporting are met.

In contrary to previously reported dose overestimation at shallow depths of up to 13% [31–33] for Tomotherapy's dose calculation algorithm in the build-up region, the results of this work show good agreement between measured and planned doses within ±4% for the target and parotid spots.

The dosimeter spots representing the eye lenses (LeL and LeR) were located in-field but direct exposure was suppressed during treatment planning. As seen in Figure 4, the TPS obviously underestimated the dose to the lens spots (LeR, LeL) in all three scenarios. At these spots, EPR measurements were in good agreement with the TLD results (Table 4 and Figure 4) and the estimated uncertainty margins for the measured and planned dose values (cf. Table 4) did not overlap, whereas no systematic dose under- or overestimation was observed for the thyroid spots lying out-of-field. Possible explanations are that Accuray's convolution/superposition dose calculation algorithm for tomotherapy neglects electron contamination, MLC transmission and dose contributions from scattered photons or secondary particles originating from closed MLC leafs [34,35]. While such dose contributions are marginal (e.g. leaf transmission is about 0.3% of the primary radiation [36]) and can be neglected for target locations receiving high doses and facing open leafs, this additional radiation may lead to considerable relative dose contributions in regions that are spared from primary beam incidence – especially when lying near to the surface. In this work, the relative dose difference was highest for the LeL spot in SC#3 which was completely blocked (cf. Section 2.3). Remarkable dose differences between measured and planned dose values for OARs during tomotherapy treatment were already reported by other researchers: Reynders et al. performed TLD measurements in an Alderson phantom undergoing a helical tomotherapy breast treatment. For the TLDs located at OARs away from the PTV (contralateral thorax wall, contralateral lung) receiving doses below 10% of the prescribed dose, the measured doses were considerably underestimated by the TPS while the planned target doses matched the measured results [37]. Consequently, caution is advised when using calculated doses for radiation risk assessments in regions of extreme OAR sparing. Further investigations regarding the root cause of the observed discrepancies were beyond the scope of the present work.

As it can be seen from Table 2 and Table 4 and from the results shown in Figure 4, the main advantage of using LFM pellets is related to the relative dose uncertainty. While both, ALA and LFM have comparable low relative dose uncertainties in the order of 0.7–0.9% (1σ) at high doses (>30 Gy), a high level of precision can be maintained at lower doses when using LFM dosimeters (rel. combined uncertainty <2% (1σ) for doses >2 Gy relative to calibrated ionization chamber dose measurements). It is a well-known characteristic of EPR

dosimetry that relative uncertainties increase with decreasing dose in the therapy dose range [38]. This is due to a constant, i.e. dose independent, uncertainty contribution that dominates the relative uncertainty at low doses. For LFM, this contribution expressed in terms of absolute dose is smaller since EPR signal intensities are higher compared to ALA. The higher EPR signal intensities result from intrinsic EPR properties (smaller spectral width) and the doubled volume of the LFM pellets. The larger longitudinal extent of the LFM pellets lead to another advantage for in vivo dosimetry: The determination of the planned dose (Section 2.5) is more reliable for LFM than for ALA and TLD, i.e. more robust against contouring errors or longitudinal misplacements (IEC y-direction). Both beneficial facts are reflected by the decreased uncertainty margins for LFM (compared to ALA) in Figure 4 at the lens and thyroid spots (low dose, high relative dose gradients).

The limitation of IVD using point detectors is that the absorbed dose is determined only at single or few points and that the dosimeter reading is sensitive to positional variations – especially in IMRT where steep dose gradients in the vicinity of the PTV are expected. The IMRT treatments performed in this work were applied to a rigid phantom geometry. While in scenario SC#1 the dosimeters were irradiated at the same position as planned, the dosimeters were repositioned between fractions in scenarios SC#2 and SC#3. During repositioning, a maximum isotropic positional tolerance of ± 2 mm was met. Positional inaccuracies were neglected in the uncertainty analysis (Table 2). By comparing the dose differences shown in Figure 4 for SC#1 to the respective values observed for SC#2, it is seen that repositioning of the dosimeters within the above mentioned tolerance did not have a remarkable impact on the result for the dosimeter spots investigated in this work. However, accurate dosimeter positioning is a crucial prerequisite for EPR in vivo dose verification as already shown by Wagner et al. [39] for head and neck cancer patients.

In this study, a practical EPR dosimetry system was validated as IVD tool to measure and verify total doses applied in realistic IMRT scenarios. The EPR dosimetry procedure is tailored for routine use featuring a measurement time of 10 min per pellet [19]. A rigid anthropomorphic phantom was used in order to verify the dosimetric procedure against TLD measurements. Patient related uncertainties due to deformable body surfaces and anatomical changes could thereby be excluded. Future EPR dosimetry studies may assess the dosimetric impact of these patient related uncertainties. EPR dosimetry is considered to be particularly useful for IVD of superficial total target doses, e.g. when bolus material is applied. Moreover, IVD at field junctions or pacemakers as well as out-of-field measurements are promising fields of application. Although in this study the EPR dosimeters were read out once after treatment was finished, earlier and repetitive evaluations are principally possible with EPR dosimetry since the dose readout is non-destructive. By this means, dosimetric verification of ongoing treatments is feasible. Finally, EPR dosimetry may provide an independent treatment record confirming that dose delivery was within expected tolerances.

Clinical implementation of EPR-IVD may be a valuable tool owing to low fading rates, superficial applicability and high levels of precision for a wide dose range – especially when using LFM dosimeters.

5 Conclusion

The present study shows that superficial in vivo EPR dosimetry is suitable for measuring and verification of total doses delivered during complex IMRT treatments for all cases considered.

EPR-IVD in this work was performed with two different dosimeter materials: Self-pressed LFM and commercial ALA pellets. Due to their higher robustness regarding contouring errors and misplacements as well as higher levels of precision at lower doses, the LFM pellets used in this work are preferable for IVD compared to commercial ALA pellets.

Relevant differences between measured and planned total doses in the order of current reporting thresholds for significant occurrences (10%/4 Gy) can be reliably detected by superficial EPR dosimetry and, thus, superficial EPR-IVD may serve as an additional safeguard during the delivery of complex IMRT treatments in the future.

Conflict of interest

All authors disclose any potential conflict of interest.

Acknowledgements

The authors would like to thank Rolf-Dieter Eckert from PTW Freiburg GmbH for the nice collaboration and multiple discussions. Special thanks to Prof. Dr. med. Stephan Mose, Dipl.-Ing. Manfred Alraun and Dipl.-Phys. Christian Albrecht from the Klinik für Strahlentherapie und Radioonkologie at the Schwarzwald-Baar Klinikum in Villingen-Schwenningen for lending us their Alderson phantom. Last but not least, we are grateful to our medical physics team including Corinna Kirchner, Tanja Hertel, Michael Schempp and Martin v. Bischopinck for careful dosimeter handling and phantom irradiations.

References

[1] International Atomic Energy Agency. Accuracy requirements and uncertainties in radiotherapy, human health series no. 31. Vienna: IAEA; 2016.

[2] Kry SF, Bednarz B, Howell RM, Dauer L, Followill D, Klein E, et al. AAPM TG 158: measurement and calculation of doses outside the treated volume from external-beam radiation therapy. Med Phys 2017;44:e391–429, http://dx.doi.org/10.1002/mp.12462.

[3] World Health Organization. Radiotherapy risk profile. Geneva: WHO Press; 2008.

[4] International Atomic Energy Agency. Investigation of an accidental exposure of radiotherapy patients in Panama: report of a team of experts. Vienna: IAEA; 2001.

[5] International Commission on Radiological Protection. Prevention of accidents to patients undergoing radiation therapy, ICRP publication 86. Bethesda, MD: ICRP; 2000.

[6] International Atomic Energy Agency. Development of procedures for in vivo dosimetry in radiotherapy, human health reports no. 8. Vienna: IAEA; 2013.

[7] Van Dam J, Marinello G. Methods for in vivo dosimetry in external radiotherapy, ESTRO booklet no. 1. 2nd ed. Brussels: European Society for Radiation Oncology, ESTRO; 2006.

[8] Richtlinie 2013/59/Euratom vom 5. Dezember 2013 zur Festlegung grundlegender Sicherheitsnormen für den Schutz vor den Gefahren einer Exposition gegenüber ionisierender Strahlung und zur Aufhebung der Richtlinien 89/618/Euratom, 90/641/Euratom, 96/29/Euratom, 97/43/Euratom und 2003/122/Euratom, Amtsblatt der Europäischen Union L13/1 vom 17.01.2014.

[9] Gesetz zum Schutz vor der schädlichen Wirkung ionisierender Strahlung vom 27. Juni 2017 (BGBl. 2017 I S. 1966).

[10] Verordnung zum Schutz vor der schädlichen Wirkung ionisierender Strahlung vom 29. November 2018 (BGBl. 2018 I S. 2034, 2036).

[11] Baffa O, Kinoshita A. Clinical applications of alanine/electron spin resonance dosimetry. Radiat Environ Biophys 2014;53:233–40, http://dx.doi.org/10.1007/s00411-013-0509-2.

[12] Indovina PL, Benassi M, Giacco GC, Primavera A, Rosati A. In vivo ESR dosimetry in total body irradiation. Strahlenther Onkol 1989;165:611–6.

[13] Kudynski R, Kudynska J, Buckmaster HA. The application of EPR dosimetry for radiotherapy and radiation protection. Appl Radiat Isot 1993;44:903–6, http://dx.doi.org/10.1016/0969-8043(93)90042-9.

[14] Kuntz F, Pabst JY, Delpech JP, Wagner JP, Marchioni E. Alanine-ESR in vivo dosimetry: a feasibility study and possible applications. Appl Radiat Isot 1996;47:1183–8.

[15] Schaeken B, Scalliet P. One year of experience with alanine dosimetry in radiotherapy. Appl Radiat Isot 1996;47:1177–82, http://dx.doi.org/10.1016/S0969-8043(96)00040-1.

[16] Wagner D, Anton M, Vorwerk H, Gsänger T, Christiansen H, Poppe B, et al. In vivo alanine/electron spin resonance (ESR) dosimetry in radiotherapy of prostate cancer: a feasibility study. Radiother Oncol 2008;88:140–7, http://dx.doi.org/10.1016/j.radonc.2008.03.017.

[17] Rech AB, Barbi GL, Ventura LHA, Guimarães FS, Oliveira HF, Baffa O. In vivo dose evaluation during gynaecological radiotherapy using L-alanine/ESR dosimetry. Radiat Prot Dosimetry 2014;159:194–8, http://dx.doi.org/10.1093/rpd/ncu128.

[18] Wagner DM, Hüttenrauch P, Anton M, von Voigts-Rhetz P, Zink K, Wolff HA. Feasibility study of entrance and exit dose measurements at the contra lateral breast with alanine/electron spin resonance dosimetry in volumetric modulated radiotherapy of breast cancer. Phys Med Biol 2017;62:5462–72, http://dx.doi.org/10.1088/1361-6560/aa6ee2.

[19] Höfel S, Stehle M, Zwicker F, Fix MK, Drescher M. A practical EPR dosimetry system for routine use in radiotherapy: uncertainty analysis of lithium formate dosimeters at the therapeutic dose level. Phys Med Biol 2021;66:045005, http://dx.doi.org/10.1088/1361-6560/ab9414.

[20] Netherlands Commission on Radiation Dosimetry. Quality assurance for tomotherapy systems, report 27. NCS; 2017, http://dx.doi.org/10.25030/ncs-027.

[21] Langen KM, Papanikolaou N, Balog J, Crilly R, Followill D, Goddu SM, et al. QA for helical tomotherapy: report of the AAPM Task Group 148. Med Phys 2010;37:4817–53, http://dx.doi.org/10.1118/1.3462971.

[22] Agostinelli S, Allison J, Amako K, Apostolakis J, Araujo H, Arce P, et al. Geant4 – a simulation toolkit. Nucl Instrum Methods Phys Res Sect A: Accel Spectrom Detect Assoc Equip 2003;506:250–303, http://dx.doi.org/10.1016/S0168-9002(03)01368-8.

[23] Sterpin E, Tomsej M, Cravens B, Salvat F, Ruchala K, Olivera GH, et al. Monte Carlo simulation of the Tomotherapy treatment unit in the static mode using MC HAMMER, a Monte Carlo tool dedicated to Tomotherapy. J Phys: Conf Ser 2007;74:021019, http://dx.doi.org/10.1088/1742-6596/74/1/021019.

[24] Sterpin E, Salvat F, Cravens R, Ruchala K, Olivera GH, Vynckier S. Monte Carlo simulation of helical tomotherapy with PENELOPE. Phys Med Biol 2008;53:2161–80, http://dx.doi.org/10.1088/0031-9155/53/8/011.

[25] BIPM, IEC, IFCC, ILAC, ISO, IUPAC, IUPAP and OIML, Evaluation of Measurement Data—Guide to the Expression of Uncertainty in Measurement JCGM 100:2008. https://www.bipm.org/utils/common/documents/jcgm/JCGM_100_2008_E.pdf.

[26] Schneider U, Hälg RA, Hartmann M, Mack A, Storelli F, Joosten A, et al. Accuracy of out-of-field dose calculation of tomotherapy and cyberknife treatment planning systems: a dosimetric study. Zeit Med Phys 2014;24:211–5, http://dx.doi.org/10.1016/j.zemedi.2013.10.008.

[27] Desrosiers MF, Puhl JM, Cooper SL. An absorbed-dose/dose-rate dependence for the alanine-EPR dosimetry system and its implications in high-dose ionizing radiation metrology. J Res Natl Inst Stand Technol 2008;113.

[28] Gustafsson H, Lund E, Olsson S. Lithium formate EPR dosimetry for verifications of planned dose distributions prior to intensity-modulated radiation therapy. Phys Med Biol 2008;53:4667, http://dx.doi.org/10.1088/0031-9155/53/17/014.

[29] Waldeland E, Malinen E. Review of the dose-to-water energy dependence of alanine and lithium formate EPR dosimeters and LiF TL-dosimeters – comparison with Monte Carlo simulations. Radiat Meas 2011;46:945–51, http://dx.doi.org/10.1016/j.radmeas.2011.03.014.

[30] Anton M, Kapsch R-P, Krauss A, von Voigts-Rhetz P, Zink K, McEwen M. Difference in the relative response of the alanine dosimeter to megavoltage X-ray and electron beams. Phys Med Biol 2013;58:3259, http://dx.doi.org/10.1088/0031-9155/58/10/3259.

[31] Ramsey CR, Seibert RM, Robison B, Mitchell M. Helical tomotherapy superficial dose measurements. Med Phys 2007;34:3286–93, http://dx.doi.org/10.1118/1.2757000.

[32] Cheek D, Gibbons JP, Rosen II, Hogstrom KR. Accuracy of TomoTherapy treatments for superficial target volumes. Med Phys 2008;35:3565–73, http://dx.doi.org/10.1118/1.2952362.

[33] Avanzo M, Drigo A, Ren Kaiser S, Roggio A, Sartor G, Chiovati P, et al. Dose to the skin in helical tomotherapy: results of in vivo measurements with radiochromic films. Phys Med 2013;29:304–11, http://dx.doi.org/10.1016/j.ejmp.2012.04.004.

[34] Accuray Inc. Physics essentials guide, 1054084-ENG A; 2017.

[35] Accuray Inc. Leaf filter theory, ETT. 700462.A; 2013.

[36] Kinhikar RA. Multileaf collimator transmission from the first Hi-Art II helical tomotherapy machine in India. J Cancer Res Ther 2008;4:88–90.

[37] Reynders T, Tournel K, De Coninck P, Heymann S, Vinh-Hung V, Van Parijs H, et al. Dosimetric assessment of static and helical TomoTherapy in the clinical implementation of breast cancer treatments. Radiother Oncol 2009;93:71–9, http://dx.doi.org/10.1016/j.radonc.2009.07.005.

[38] Anton M. Uncertainties in alanine/ESR dosimetry at the Physikalisch-Technische Bundesanstalt. Phys Med Biol 2006;51:5419–40, http://dx.doi.org/10.1088/0031-9155/51/21/003.

[39] Wagner D, Anton M, Vorwerk H. Dose uncertainty in radiotherapy of patients with head and neck cancer measured by in vivo ESR/alanine dosimetry using a mouthpiece. Phys Med Biol 2011;56:1373–83, http://dx.doi.org/10.1088/0031-9155/56/5/010.